Supplementary Information

Boosting Efficiency and Stability of $CuBi_2O_4$ Photocathodes Achieved through Template Engineering and FeOOH Modification

Ying Wang [†, ‡], Hao Zhang[‡], Qitao Liu [‡] and Yongbo Kuang*[‡, ⁋]

† Institute of Materials, Ningbo University of Technology, Ningbo 315211, China

‡ Zhejiang Key Laboratory of Advanced Fuel Cells and Electrolyzers Technology, Ningbo Institute of Materials Technology and Engineering, Chinese Academy of Sciences, Ningbo 315201, China

E-mail: kuangyongbo@nimte.ac.cn

⁋ Center of Materials Science and Optoelectronics Engineering, University of Chinese Academy of Sciences, Beijing 100049, China

E-mail: kuangyongbo@nimte.ac.cn

Materials and methods

Materials: Copper acetate ($Cu(C_2H_3O_2)_2 \cdot H_2O$), sodium acetate ($CH_3COONa$), sodium hydroxide (NaOH), bismuth hydroxide ($Bi(OH)_3$), potassium chloride (KCl), ferrous sulfate ($FeSO_4 \cdot 7H_2O$), potassium hydroxide (KOH), boric acid (H_3BO_3), and hydrogen peroxide (H_2O_2) were of analytical grade and used as received without further purification. Fluorine-doped tin oxide (FTO) glass substrates were sequentially cleaned by sonication in detergent, deionized water, acetone, and ethanol, followed by drying under N_2. Unless otherwise stated, the geometric working area of the working electrode was defined as 0.5 cm^2 by masking the surrounding area with chemically resistant tape.

Overall fabrication strategy. CBO thin-film photocathodes were prepared via a two-step route that decouples the Cu and Bi sources. First, an electrodeposited Cu_2O thin film on a conductive substrate (FTO) served as the Cu precursor. Next, $Bi(OH)_3$ was introduced by dip-coating to provide a conformal Bi source. A subsequent annealing step drives the solid-state reaction between Cu_2O and $Bi(OH)_3$, ultimately yielding the CBO thin-film photocathode.

Electrodeposition of (111)-Cu_2O Template: For the preparation of the Cu_2O thin films, electrochemical deposition was carried out in an electrolyte containing 0.1 M copper acetate and 0.1 M sodium acetate, with the pH adjusted to 5. FTO-coated glass, a Pt foil, and an Ag/AgCl electrode were used as the working, counter, and reference electrodes, respectively. The deposition was conducted in a glass cell with an electrolyte volume of ~100 mL at ~60 °C. Deposition was performed at a constant

potential of -0.23 V for 180 s. After deposition, the electrodes were rinsed with deionized water and dried under nitrogen.

Synthesis of CBO Photocathodes: The obtained Cu_2O films were then immersed in a 0.1 M $Bi(OH)_3$ suspension and coated using a dip-coating method. The coating speed was set to 5 mm min^{-1}, with three coating cycles (or a single cycle using a 0.5 M suspension). After drying in air, the samples were annealed in a tube furnace under ambient atmosphere at 500 °C for 2 h, using a heating rate of 5 °C min^{-1}. This annealing treatment induced the solid-state reaction between Cu_2O and $Bi(OH)_3$, transforming the precursor layers into the CBO thin film. The films were then naturally cooled to room temperature. CBO electrodes with different film qualities were further prepared by varying the number of dip-coating cycles (one to five cycles) and the concentration of the Bi precursor suspension (0.1~0.5 M).

Galvanostatic Deposition of FeOOH: FeOOH cocatalysts were deposited onto the CBO photocathodes via a photoelectrochemical (PEC) deposition route. A three-electrode cell was employed, comprising the CBO-coated substrate as the working electrode, a Pt counter electrode, and an Ag/AgCl reference electrode, all connected to a potentiostat. The deposition electrolyte was freshly prepared by dissolving 5 mM $FeSO_4 \cdot 7H_2O$ in 60 mL of 0.1 M K_2SO_4 at 70 °C, without additional pH adjustment. To suppress Fe^{2+} oxidation and minimize interference from dissolved oxygen, the solution was purged with N_2 for 30 min prior to deposition, and the CBO working electrode was maintained under an N_2 atmosphere. Galvanostatic deposition was then conducted at a constant current of 0.1 mA for 60 s with gentle magnetic stirring to ensure uniform

mass transport. After deposition, the electrode was immediately withdrawn, thoroughly rinsed with deionized water to remove residual electrolyte, and optionally immersed in deionized water or a pH-controlled buffer for post-treatment. Finally, the samples were dried using air drying, N_2 blowing, mild oven drying (40-80 °C), or vacuum drying, as specified for subsequent characterization and PEC measurements.

Characterization. X-ray diffraction (XRD) patterns of all the samples were collected using a Rigaku Smartlab X-Ray Diffractometer operated with a Cu Kα radiation source at 40 kV and 30 mA. The morphologies and elemental distribution of the samples were recorded using a Hitachi S4800 Scanning Electron Microscope (SEM) and EDX operated at 20 kV. Transmission electron microscopy (TEM) study of the samples was performed using a Tecnai F20 instrument with an acceleration voltage of 200 kV. The light harvesting performance was obtained by UV-visible spectrophotometer with an integrating sphere (Perkin-Elmer Lambda 950). The chemical state of the as-prepared samples was investigated using X-ray photoelectron spectroscopy through Mg Ka radiation (1253.6 eV) on an ESCA MULTIPLEX-1600. The UPS measurements were performed using a He I (21.22 eV) excitation line, and the work function was determined from the UPS spectra by subtracting their width (that is, the energy difference between the analyser Fermi level and the high binding energy cut-off), from the He I excitation energy.

Electrochemical and photoelectrochemical (PEC) measurements. The electrochemical (EC) and photoelectrochemical (PEC) performances of CBO based photocathodes were measured with a three-electrode configuration using a CHI660

potentiostat, a saturated Ag/AgCl ($E_{Ag/AgCl}$ = 0.197 V versus NHE at 25 ºC) reference electrode and a Pt wire counter electrode. The recorded potentials versus Ag/AgCl ($E_{vs. Ag/AgCl}$) were converted against reversible hydrogen electrode (RHE) using the Nernst equation ($E_{vs. RHE} = E_{vs. Ag/AgCl}+E_{Ag/AgCl}+0.059pH$). The electrolyte comprised a pH 9 H_3BO_3-KOH buffer solution (0.5 M H_3BO_3), with the addition of 0.3 M H_2O_2 as an electron scavenger, and its pH was accurately measured using a pH meter. Illumination was provided by a monochromatic blue LED (39 mW cm^{-2}, λ = 455 nm), directing light through glass onto the FTO/CBO electrode *via* backside illumination. All experiments were performed at a controlled temperature of 25 ± 2 °C. LSV was performed with a negative potential scan direction at a scan rate of 10 mV s^{-1}. CA measurements were carried out at 0.6 V_{RHE}. The incident-photon-to-current efficiency (IPCE) was performed under monochromatic light using bandpass filters and calculated as follows,

$$IPCE = \frac{1240(V \cdot nm) \cdot i(mA/cm^2)}{P_\lambda(mW/cm^2) \cdot \lambda(nm)} \quad (1)$$

where 1240 (V·nm) is a multiplication of *h* (Planck's constant) and *c* (the speed of light), *i* (mA·cm-2) is the photocurrent density, λ (nm) is the wavelength of incident photon, and P_λ (mW·cm-2) is the light intensity at λ. P_λ was measured with a photometer. The photocurrent density, *i*, was determined by measuring current versus time curve at a constant potential (0.6 V_{RHE}).

Electrochemical impedance spectroscopy (EIS) was performed using a Solartron Modulab XM potentiostat over a frequency range from 0.1 Hz to 100 kHz with an

amplitude of 10 mV. Measurements were conducted at constant potentials of 0.6 V_{RHE}.

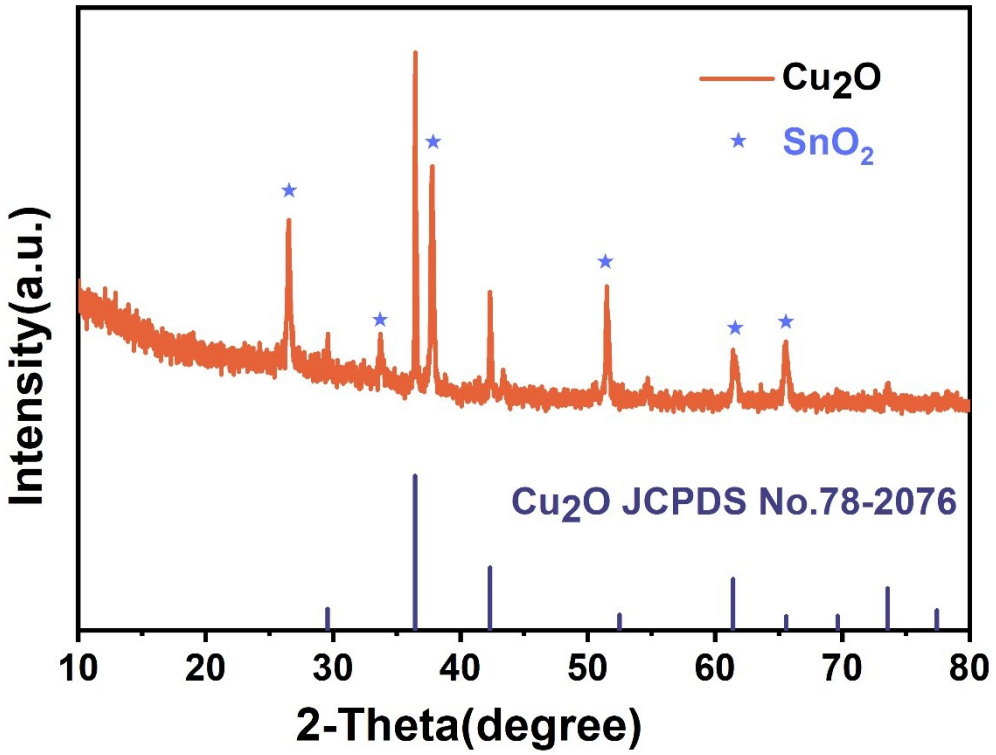

Figure S1. XRD patterns for Cu_2O templates.

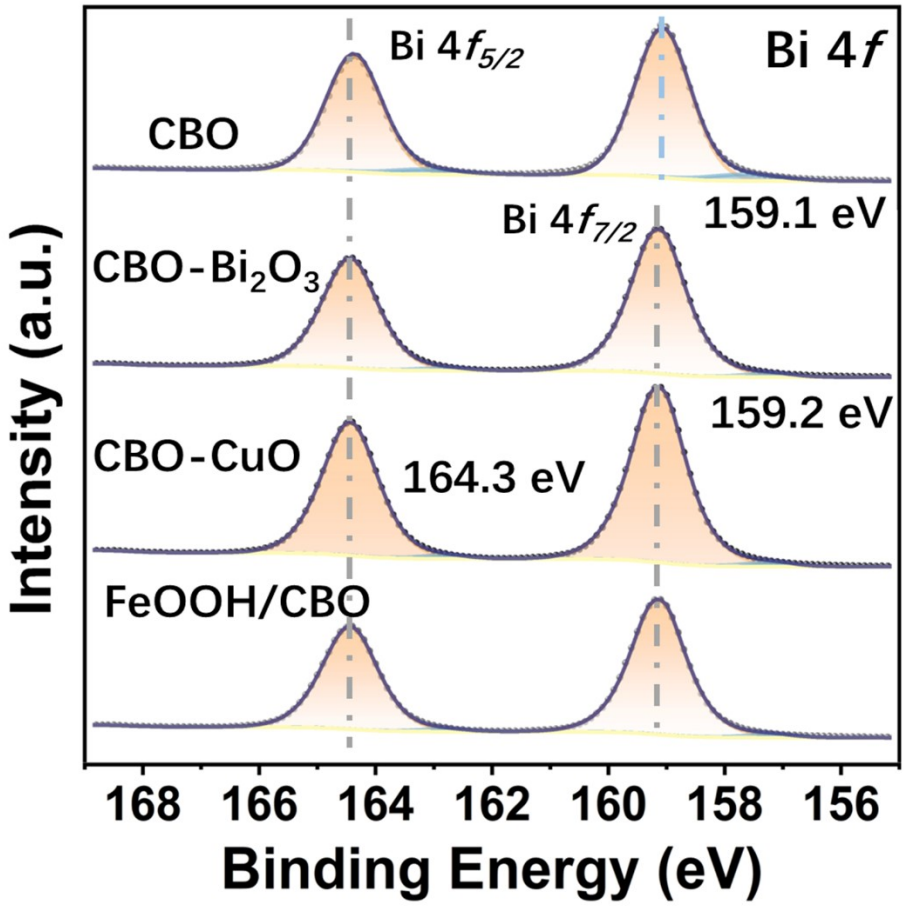

Figure S2. XPS spectra of Bi 4f for CBO, CBO-CuO, CBO-Bi_2O_3 and FeOOH/CBO.

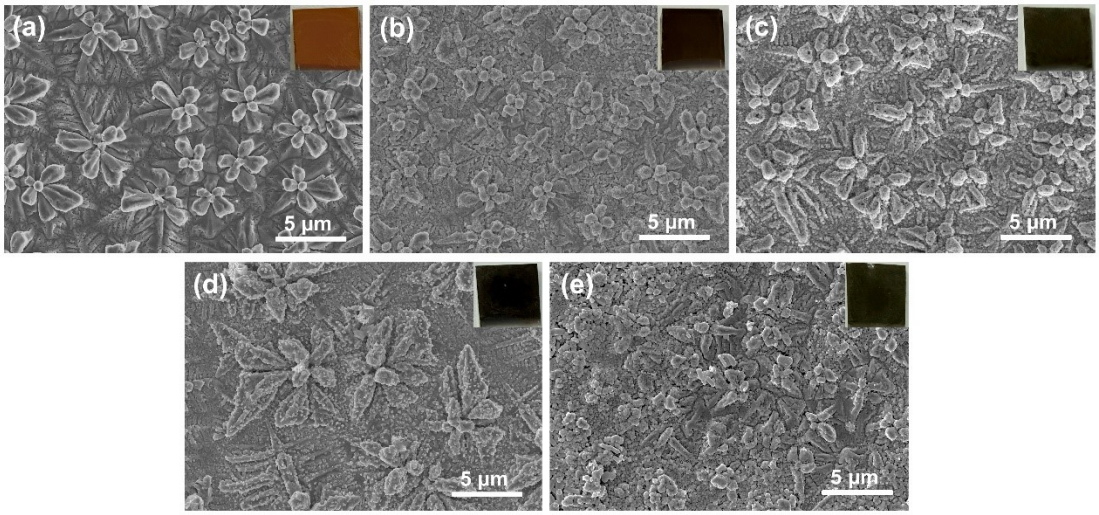

Figure S3. The low-magnification SEM micrographs for (a) Cu_2O templates, (b) CBO, (c) FeOOH/CBO, (d) CBO-CuO and (e) CBO-Bi_2O_3, the inset figures are the corresponding real photos for the different samples.

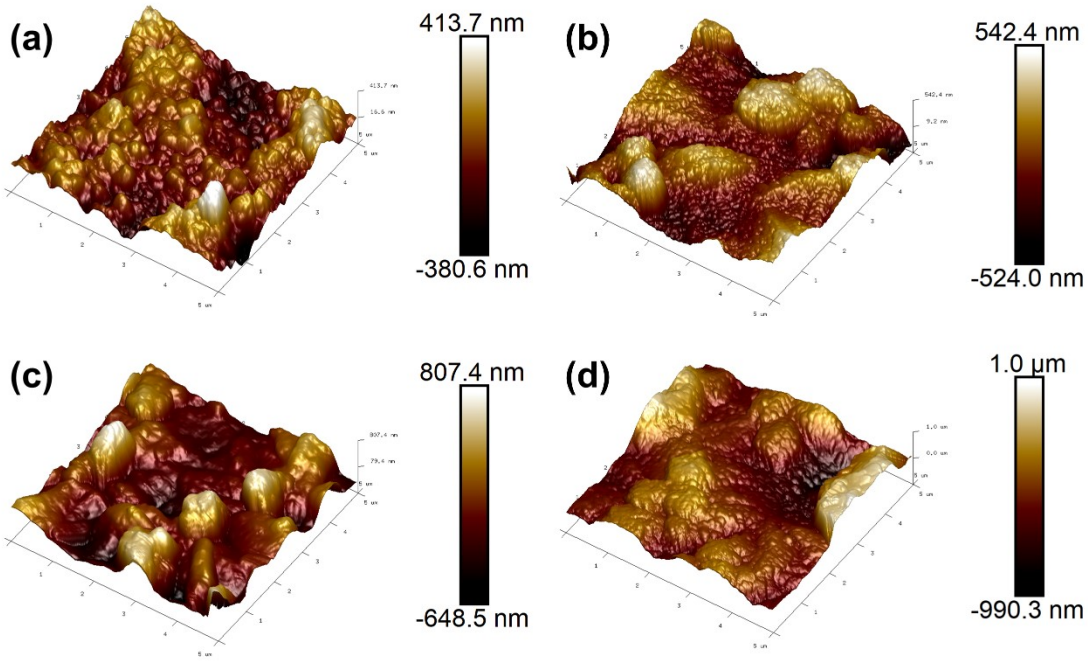

Figure S4. The roughness measurements for (a) CBO-Bi_2O_3, (b) CBO, (c) CBO-CuO, and (d) FeOOH/CBO.

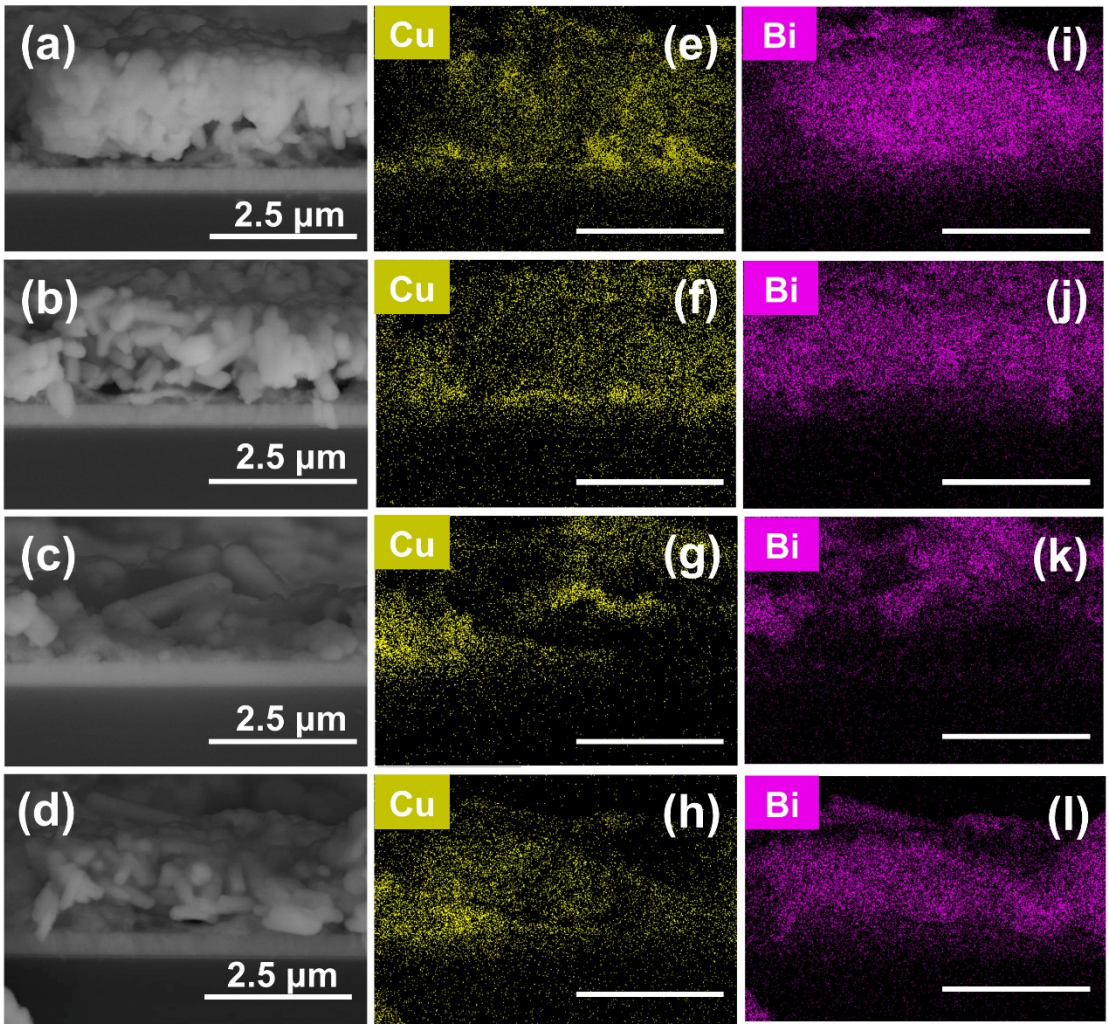

Figure S5. Cross-sectional SEM-EDS analyses for (a), (e) and (i) CBO-Bi_2O_3, (b), (f) and (j) CBO, (c), (g) and (k) CBO-CuO, (d), (h) and (l) FeOOH/CBO.

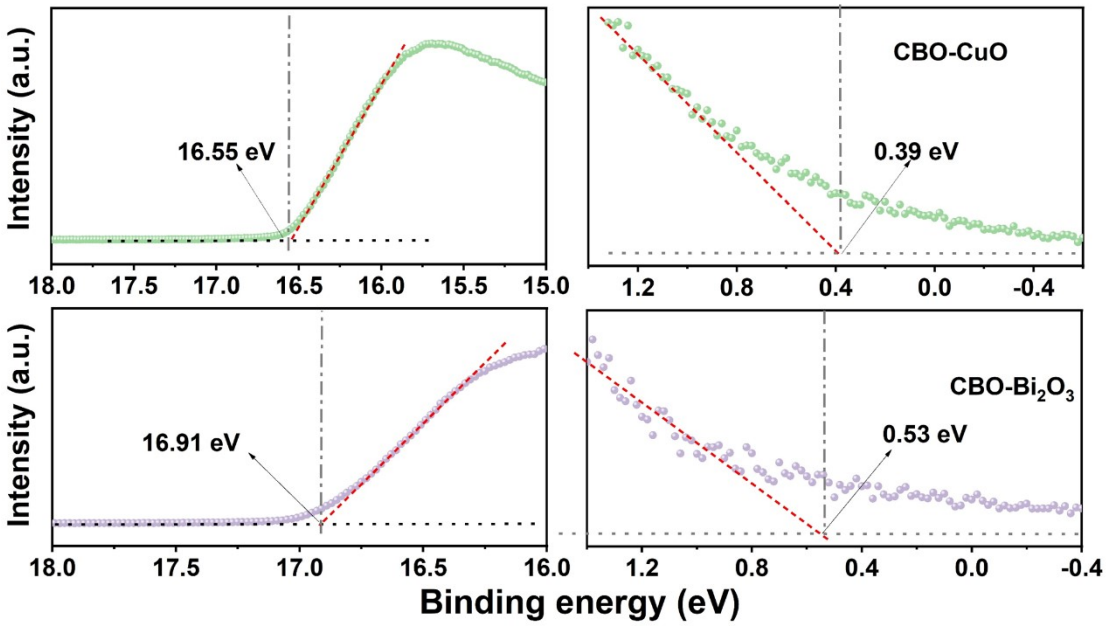

Figure S6. UPS spectra which illustrate the valence band region and work function information for CBO-CuO and CBO-Bi_2O_3.

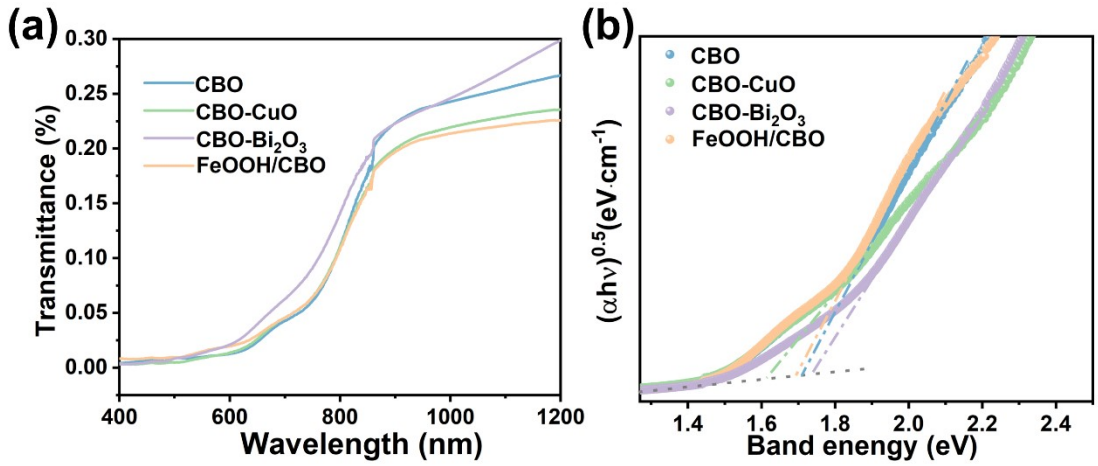

Figure S7. (a) UV-Vis transmittance spectra and (b) the corresponding optical band gap plots derived from the transmittance spectra for different CBO thin film electrodes.

Table S1. EIS fitting parameters for different CBO thin film electrodes in an aqueous KOH/H_3BO_3 (0.5 M, pH 9.0) buffer under illumination at a potential bias of 0.6 V_{RHE}.

Samples	$R_1(\Omega)$	$R_2(\Omega)$	$R_3(\Omega)$	CPE-1(F)	CPE-2(F)
CBO	60.5	255.6	45.5	4.4×10^{-4}	1.5×10^{-5}
CBO-Bi_2O_3	66.1	390.9	35.5	6.0×10^{-5}	1.5×10^{-6}
CBO-CuO	60.9	349.2	23.5	1.6×10^{-5}	1.5×10^{-6}
FeOOH/CBO	51.9	230.9	1.5	2.4×10^{-5}	1.5×10^{-6}

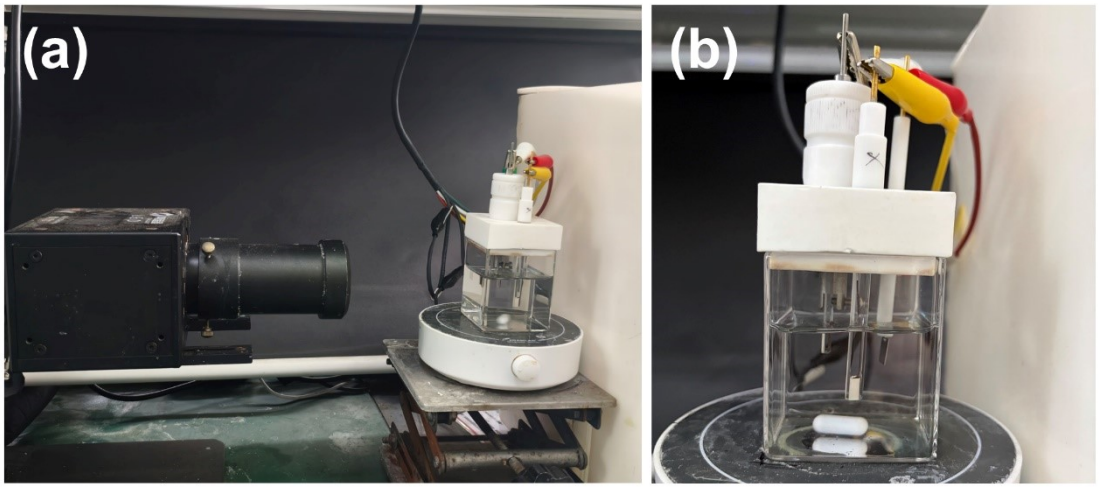

Figure S8. Photographs of (a) PEC measurement setup, (b) the sample and electrical connection configuration.

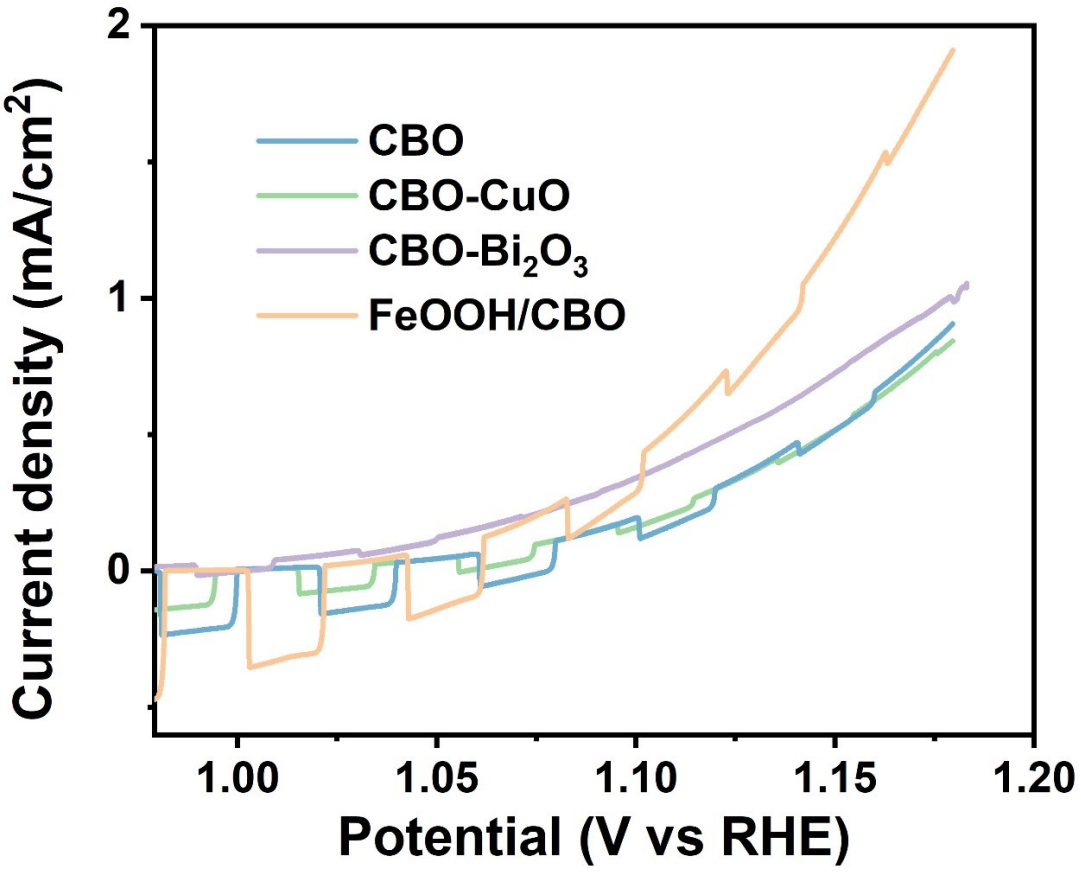

Figure S9. Magnified current-potential curves in a 0.5 M borate buffer solution (pH 9) containing 0.3 M H_2O_2 under LED irradiation (λ=455 nm, 39 mW/cm^2).

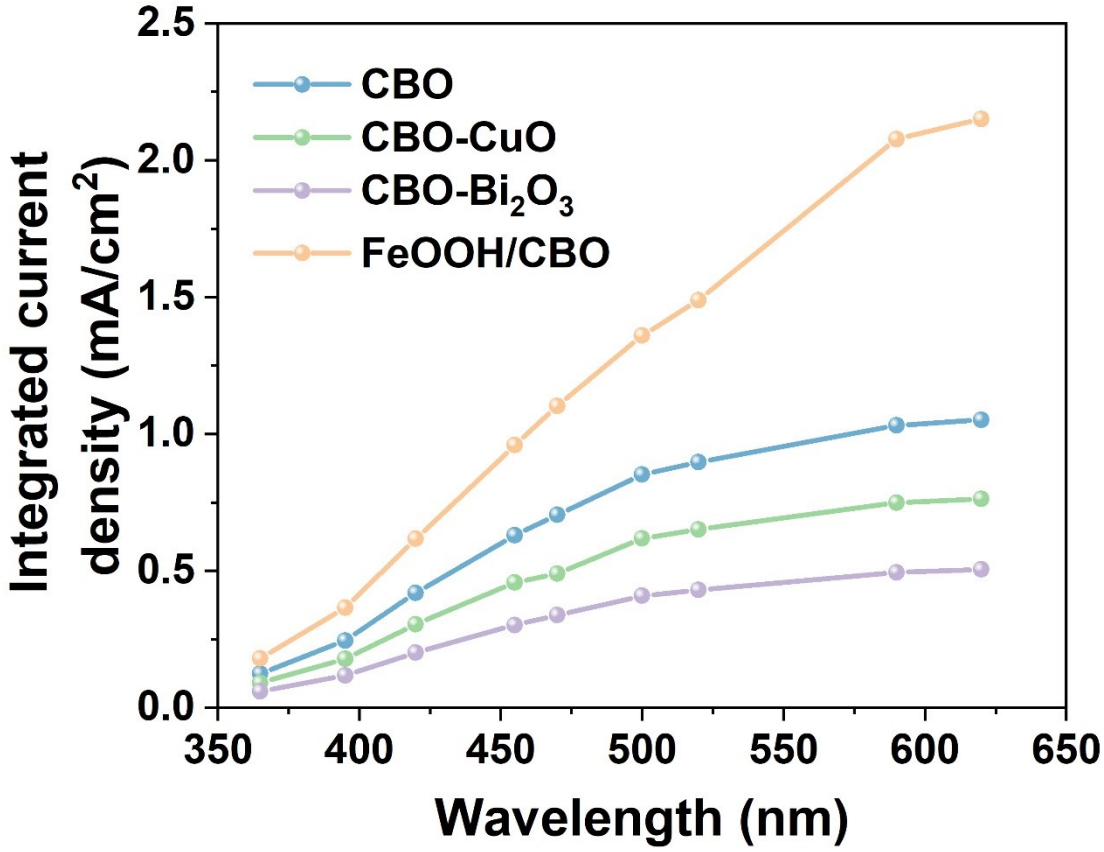

Figure S10. Integrated photocurrent densities for different CBO thin film electrodes in a 0.5 M borate buffer solution (pH 9) containing 0.3 M H_2O_2 at 0.6 V_{RHE} under irradiation.

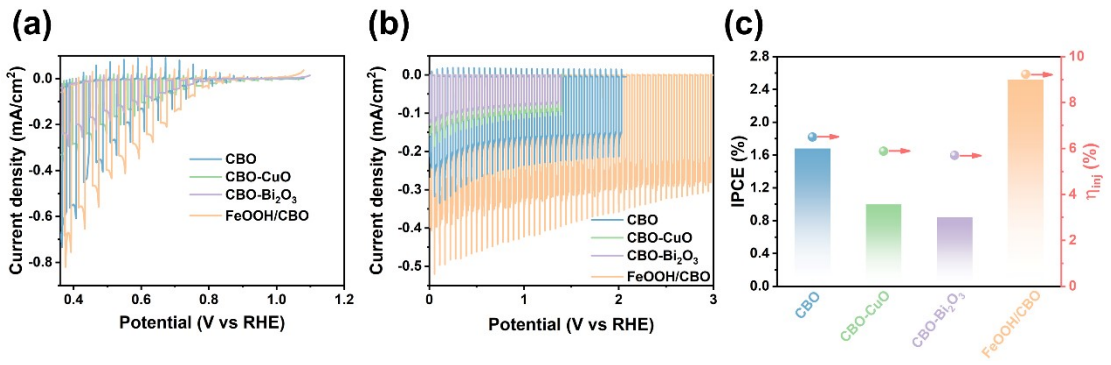

Figure S11. (a) Current-potential curves, (b) photocurrent change, (c) the IPCEs and experimentally-estimated surface transfer efficiency for the proof of calculation results at 0.6 V_{RHE} for different CBO thin film electrodes in a 0.5 M borate buffer solution (pH 9) under LED irradiation (λ=455 nm, 39 mW/cm^2).